substance: VO_2
property: effect of dopant ions on crystal structure

Two different types of aliovalent dopant have marked effects: M^{3+} and M^{5+}.

phase diagrams: $Ga_xV_{1-x}O_2$: Fig. 1, $Al_xV_{1-x}O_2$: Fig. 2, $0 \leq x \leq 0.012$ M_1-phase, $0.012 \leq x \leq 0.030$ T-phase, $0.030 \leq x \leq 0.045$ M_2-phase, $x > 0.045$ $AlVO_4$ [74D], $Fe_xV_{1-x}O_2$: Fig. 3, extended phase diagram [76K], $0.05 \leq x \leq 0.11$ M_4-phase $0.11 \leq x \leq 0.13$ orthorhombic phase, $Cr_xV_{1-x}O_2$: Fig. 4, $Ti_xV_{1-x}O_2$: Fig. 5, extended phase diagram [76H1], $0.14 \leq x \leq 0.24$ M_4-phase, $x > 0.24$ tetragonal semiconducting rutile R_s-phase, $Nb_xV_{1-x}O2$: Fig. 6.

For the M^{3+}-ion substituents, the following phases are formed:

M_1: monoclinic; isostructural with low temperature VO_2; Fig. 7.

M_2: a new monoclinic phase; schematic plan of $(110)_R$, Fig. 7 Half the V *c*-axis pairs tilt but do not pair the others pair, but do not tilt, though the V^{4+} ions are localized [76P],

T: (also referred to in earlier literature as M_3): a new triclinic phase intermediate between M_1 and M_2,

M_4: a monoclinic phase closely related to M_2 is found for larger values of x. Some long range order has disappeared compared to M_2.

$Al_{0.015}V_{0.985}O_2$

Detailed evolution of lattice parameters: Fig. 8, refined interatomic distances and effective charges: (Table from [77G])

(Phases labelled as in Fig. 2. The V(l) chains are paired along the c_R (= a_m) axis in M_2 and the V(2) chains are tilted: Fig. 7b. In the T-phase this distinction is less clearcut).

Phases:	R		M_2	T_{298K}	T_{173K}
Effective charge (in units of *e*)	3.88	V(1)	3.90	3.96	3.78
		V(2)	3.96	4.00	4.17
V – O average distances (in Å)	1.926	V(1)	1.945	1.934	1.946
		V(2)	1.946	1.935	1.921
V – V distances across the sheared face (in Å)	2.853	V(1)	2.540	2.547	2.545
			3.261	3.226	3.200
		V(2)	2.935	2.819	2.747
			2.935	3.005	3.051

$Cr_{0.024}V_{0.976}O_2$

Detailed evaluation of lattice parameters: Fig. 9, temperature-pressure diagram: Fig. 10.

$Nb_xV_{1-x}O_2$

Detailed structural investigations apparently not reported. Phase diagram (Fig. 6) shows M_1 structure which transforms into M' by loss of long-range order in $(110)_R$ and/or $(\bar{1}\ \bar{1}\ 0)_R$ planes of M_1 structure. The R' phase may similarly be derived from the rutile R phase [76P].

$W_xV_{1-x}O_2$

Monoclinic phases and tetragonal phases (for x > 0.017) also found [69N, 72H].

An increase in pressure brings about a reduction in the $M_2 \rightarrow R$ transition of $M_x^{3+}V_{1-x}O_2$ and an increase in the $T \rightarrow M_2$ transition. Above a critical pressure p_{crit} that depends on x the M_2 phase disappears and the $T \rightarrow R$ transition temperature above this pressure is independent of pressure [80T].

Compound	x	p_{crit} [kbar]	dT_{tr}/dp ($T \rightarrow M2$) [K kbar^{-1}]	dT_{tr}/dp ($M2 \rightarrow R$) [K kbar^{-1}]
$Fe_xV_{1-x}O_2$	0.00011	7.5	– 1.21	+ 3.97
	0.00015	10.5	– 1.15	+ 3.75
	0.0002	14.4	– 0.90	+ 3.47
$Ga_xV_{1-x}O_2$	0.000073	6.3	– 0.79	+ 4.29
$Al_xV_{1-x}O_2$	0.000075	6.7	– 0.75	+ 4.33
	0.00024	26.0	– 0.88	+ 1.88

(Table from [80T])

References:

69M MacChesney, J. B., Guggenheim, H. J.: J. Phys. Chem. Solids 30 (1969) 225.
69N Nygren, M., Israelsson, M.: Mater. Res. Bull. 4 (1969) 881.
71V Villeneuve, G., Bordet, A., Casalot, A., Hagenmuller, P.: Mater. Res. Bull. 6 (1971) 119.
72H Horlin, T., Niklewski, T., Nygren, M.: Mater. Res. Bull. 7 (1972) 1515.
72M Marezio, M., Mcwhan, D. B., Remeiki, J. P., Dernier, P. D.: Phys. Rev. B5 (1972) 2541.
73V Villeneuve, G., Drillon, M., Hagenmuller, P.: Mater. Res. Bull. 8 (1973) 1111.
74D Drillon, M., Villeneuve, G.: Mater. Res. Bull. 9 (1974) 1199.
74P Pouget, J. P., Launois, H., Rice, T. M., Dernier, P. D., Gossard, A., Villeneuve, G., Hagenmuller, P.: Phys. Rev. B10 (1974) 1801.
76B Brückner, W., Gerlach, U., Moldenhauer, W., Brückner, H. P., Thuss, B., Oppermann, H., Wolf, E., Storbeck, I.: J. Phys. (Paris) Colloq. 37 (1976) C463.
76H1 Hörlin, T., Niklewski, T., Nygren, M.: J. Phys. (Paris) Colloq. 37 (1976) C4-69.
76H2 Hörlin, T., Niklewski, T., Nygren, M.: Acta Chem. Scand. A30 (1976) 619.
76K Kosuge, K., Kachi, S.: Mater. Res. Bull. 11 (1976) 255.
76P Pouget, J. P., Launois, H.: J. Phys. (Paris) Colloq. 37 (1976) C4-39.
77G Ghedira, M., Vincent, H., Marezio, M., Launay, J. C.: J. Solid State Chem. 22 (1977) 423.
77V Villeneuve, G., Drillon, M., Hagenmuller, P., Nygren, M., Pouget, J. P., Carmona, F., Delhaes, P.: J. Phys. C10 (1977) 3621.
78P Pintchovskii, F., Glausinger, W. S., Navrotsky, A.: J. Phys. Chem. Solids 39 (1978) 941
80T Terukov, E. I., Orchinnikov, S. G., Zyuzui, A. Yu., Gerlach, U., Oppermann, H., Reichelt, W.: Fiz. Tverd. Tela 22 (1980) 1374.

Fig. 1.

$Ga_xV_{1-x}O_2$. Phase diagram [78P]. R: rutile (structure), M_1, M_2: monoclinic phases, T: triclinic phase.

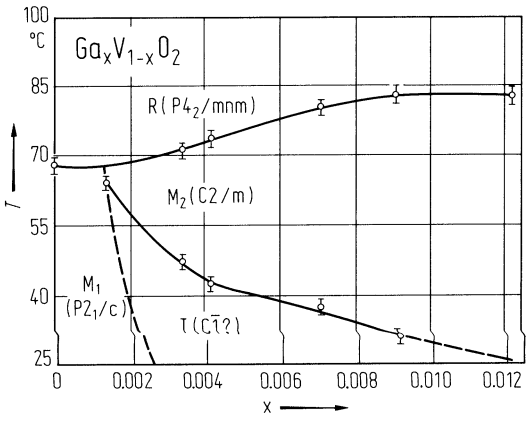

Fig. 2.

$Al_xV_{1-x}O_2$. Phase diagram [77V]. R: rutile.

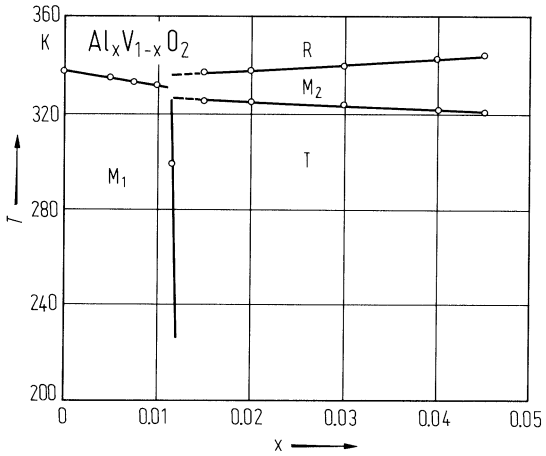

Fig. 3.

$Fe_xV_{1-x}O_2$. (a) Phase diagram, (b) hysteresis in M_2 – R transition [76B]. Circles: on heating.

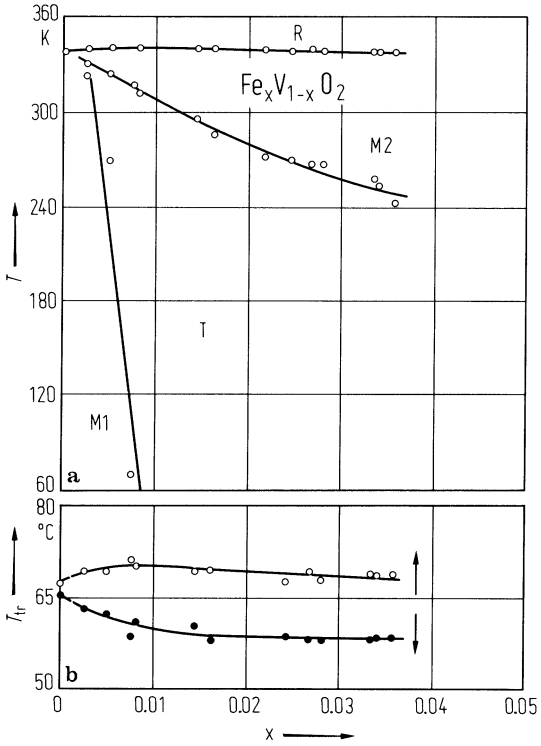

Fig. 4.

$Cr_xV_{1-x}O_2$. Phase diagram (*A* acc.to [73V], *B* acc.to [72M], [74P]).

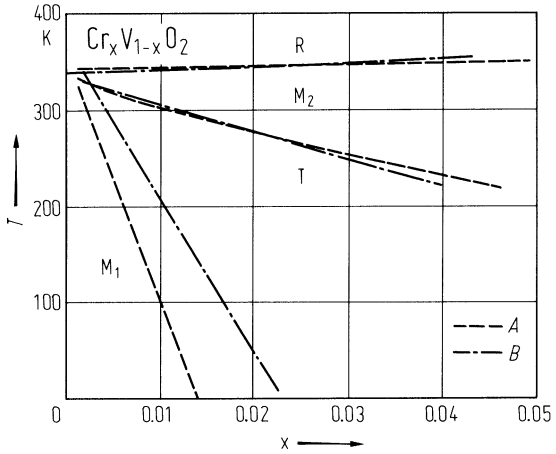

Fig. 5.

$Ti_xV_{1-x}O_2$. Phase diagram for small x [76H2].

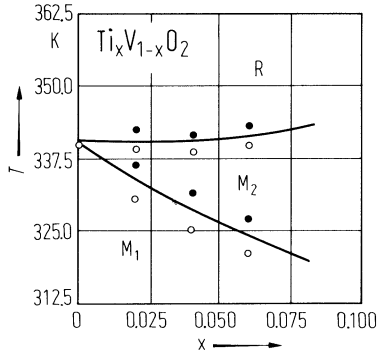

Fig. 6.

$Nb_xV_{1-x}O_2$. Phase diagram. Hatched area represents uncertainty in the broad DTA peaks [76P]. M', R' phases: see tables.

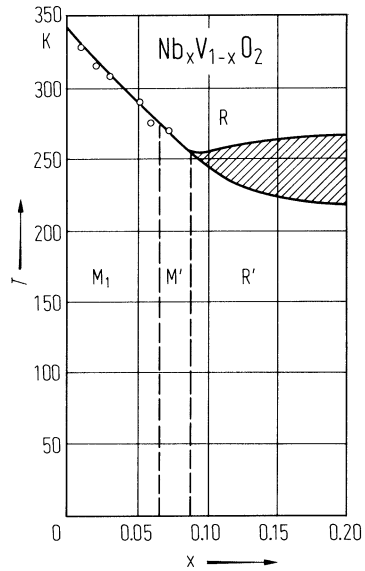

Fig. 7.

VO_2. Schematic projection of the M_1 and M_2 structures onto $[110]_R$ [74D]. + and – signs refer to V atoms above and below the plane of paper.

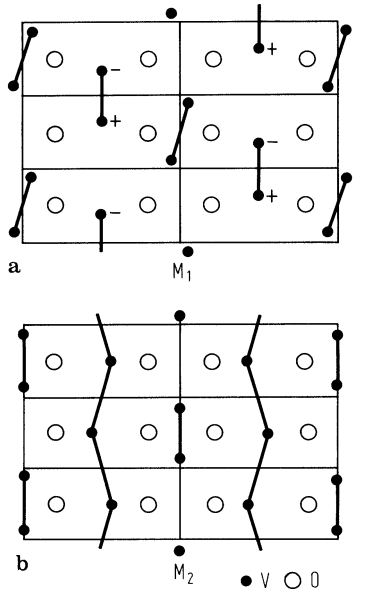

Fig. 8.

$Al_{0.015}V_{0.985}O_2$. Lattice parameters vs. temperature [77G]. R: rutile.

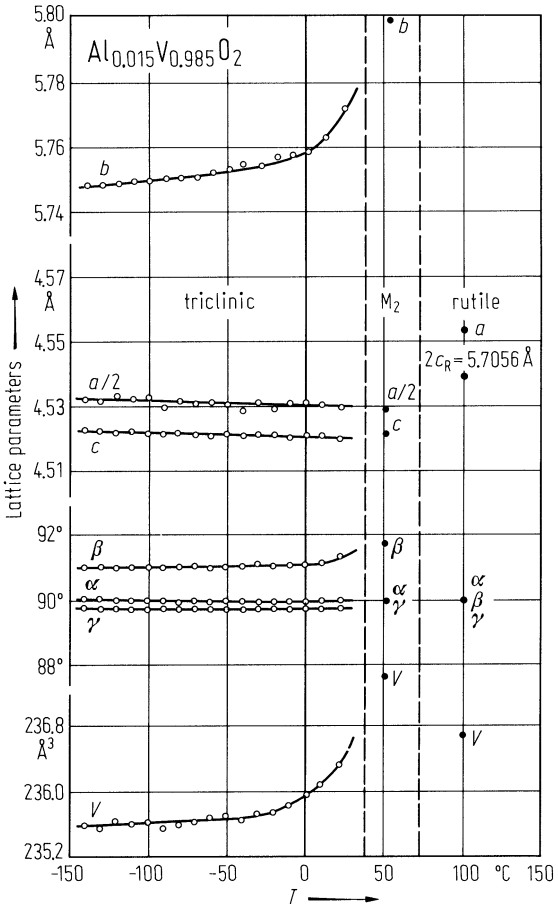

Fig. 9.

$Cr_{0.024}V_{0.976}O_2$. Lattice parameters vs. temperature [72M]. Subscript m: monoclinic.

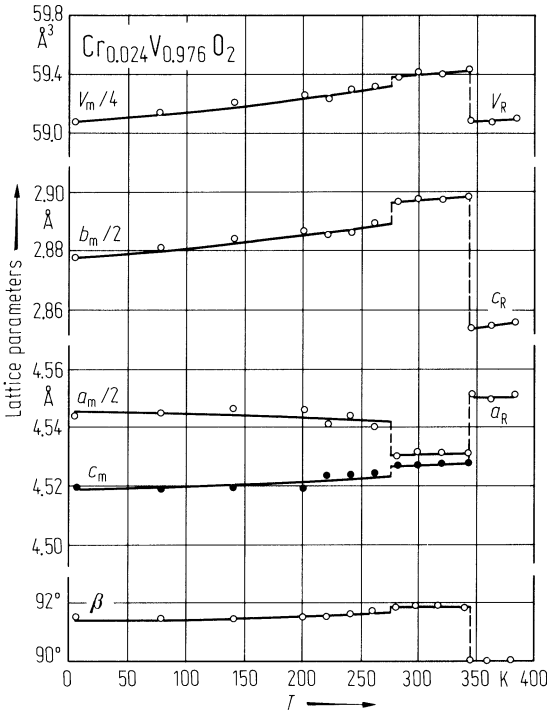

Fig. 10.

$Cr_{0.024}V_{0.976}O_2$. Phase diagram. Experimental data according to [71V], [69M], [72M].